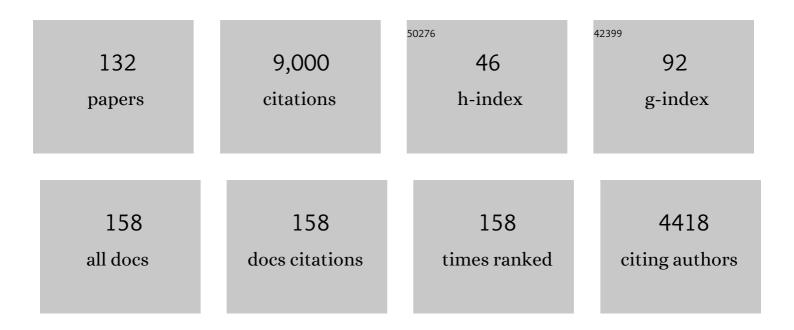
Xiaohui Yuan

List of Publications by Year in descending order

Source: https://exaly.com/author-pdf/3779924/publications.pdf Version: 2024-02-01



#	Article	IF	CITATIONS
1	Preservation of the Iberian Tethys paleomargin beneath the eastern Betic mountain range. Gondwana Research, 2022, 106, 237-246.	6.0	3
2	Crustal and uppermost mantle structure of the NW Namibia continental margin and the Walvis Ridge derived from ambient seismic noise. Geophysical Journal International, 2022, 230, 377-391.	2.4	1
3	Lateral Growth Mechanism of Protoâ€ībetan Plateau in the Late Paleogene: Implications From Detailed Crustal Structures of the Hoh Xil Basin. Geophysical Research Letters, 2022, 49, .	4.0	4
4	Intracontinental deformation of the Tianshan Orogen in response to India-Asia collision. Nature Communications, 2022, 13, .	12.8	27
5	Eastward Dipping Style of the Underthrusting Indian Lithosphere Beneath the Tethyan Himalaya Illuminated by P and S Receiver Functions. Journal of Geophysical Research: Solid Earth, 2021, 126, .	3.4	4
6	Seismic, Receiver Function Technique. Encyclopedia of Earth Sciences Series, 2021, , 1580-1592.	0.1	1
7	The Hindu Kush slab break-off as revealed by deep structure and crustal deformation. Nature Communications, 2021, 12, 1685.	12.8	39
8	Deep Crustal Contact Between the Pamir and Tarim Basin Deduced From Receiver Functions. Geophysical Research Letters, 2021, 48, e2021GL093271.	4.0	9
9	Full Waveform Inversion Beneath the Central Andes: Insight Into the Dehydration of the Nazca Slab and Delamination of the Backâ€Arc Lithosphere. Journal of Geophysical Research: Solid Earth, 2021, 126, e2021JB021984.	3.4	21
10	Seismic structure across central Myanmar from joint inversion of receiver functions and Rayleigh wave dispersion. Tectonophysics, 2021, 818, 229068.	2.2	5
11	Impact of the Juan Fernandez Ridge on the Pampean Flat Subduction Inferred From Full Waveform Inversion. Geophysical Research Letters, 2021, 48, e2021GL095509.	4.0	7
12	Backâ€Arc Extension of the Central Bransfield Basin Induced by Ridge–Trench Collision: Implications From Ambient Noise Tomography and Stress Field Inversion. Geophysical Research Letters, 2021, 48, e2021GL095032.	4.0	6
13	Structure and Stress Field of the Lithosphere Between Pamir and Tarim. Geophysical Research Letters, 2021, 48, e2021GL095413.	4.0	15
14	Moho and uppermost mantle structure in the Alpine area from S-to-P converted waves. Solid Earth, 2021, 12, 2503-2521.	2.8	7
15	Complex structure of upper mantle beneath the Yadong-Gulu rift in Tibet revealed by S-to-P converted waves. Earth and Planetary Science Letters, 2020, 531, 115954.	4.4	37
16	BRAVOSEIS: Geophysical investigation of rifting and volcanism in the Bransfield strait, Antarctica. Journal of South American Earth Sciences, 2020, 104, 102834.	1.4	16
17	Mantle Transition Zone Structure Beneath Myanmar and Its Geodynamic Implications. Geochemistry, Geophysics, Geosystems, 2020, 21, e2020GC009262.	2.5	17
18	Lateral growth of NE Tibetan Plateau restricted by the Asian lithosphere: Results from a dense seismic profile. Gondwana Research, 2020, 87, 238-247.	6.0	12

Χιαομυί Υυάν

#	Article	IF	CITATIONS
19	Lithospheric Delamination Beneath the Southern Puna Plateau Resolved by Local Earthquake Tomography. Journal of Geophysical Research: Solid Earth, 2020, 125, e2019JB019040.	3.4	9
20	Seismic discontinuities in the lithospheric mantle at the Dead Sea Transform. Geophysical Journal International, 2020, 223, 1948-1955.	2.4	1
21	Crustal Structure of Sri Lanka Derived From Joint Inversion of Surface Wave Dispersion and Receiver Functions Using a Bayesian Approach. Journal of Geophysical Research: Solid Earth, 2020, 125, e2019JB018688.	3.4	12
22	Geodynamic processes of the continental deep subduction: Constraints from the fine crustal structure beneath the Pamir plateau. Science China Earth Sciences, 2020, 63, 649-661.	5.2	5
23	Detailed Moho variations under Northeast China inferred from receiver function analyses and their tectonic implications. Physics of the Earth and Planetary Interiors, 2020, 300, 106448.	1.9	24
24	Sharp Lateral Moho Variations Across the SE Tibetan Margin and Their Implications for Plateau Growth. Journal of Geophysical Research: Solid Earth, 2020, 125, e2019JB018117.	3.4	27
25	New insights into the structural elements of the upper mantle beneath the contiguous United States from <i>S</i> -to- <i>P</i> converted seismic waves. Geophysical Journal International, 2020, 222, 646-659.	2.4	24
26	Velocity structure and radial anisotropy of the lithosphere in southern Madagascar from surface wave dispersion. Geophysical Journal International, 2020, 224, 1930-1944.	2.4	2
27	The Crust in the Pamir: Insights From Receiver Functions. Journal of Geophysical Research: Solid Earth, 2019, 124, 9313-9331.	3.4	42
28	Seismic Evidence for Lateral Asthenospheric Flow Beneath the Northeastern Tibetan Plateau Derived From S Receiver Functions. Geochemistry, Geophysics, Geosystems, 2019, 20, 883-894.	2.5	18
29	Moho Doublet in Southern Tibet and Its Tectonic Implication. Acta Geologica Sinica, 2019, 93, 43-44.	1.4	Ο
30	Seismic imaging of subduction of continental crust beneath the Pamir. Acta Geologica Sinica, 2019, 93, 65-65.	1.4	0
31	Observations of guided waves from the Pamir seismic zone provide additional evidence for the existence of subducted continental lower crust. Tectonophysics, 2019, 762, 1-16.	2.2	8
32	De-noising receiver function data using the Seislet Transform. Geophysical Journal International, 2019, 217, 2047-2055.	2.4	13
33	Imaging the Mantle Lithosphere below the China cratons using S-to-p converted waves. Tectonophysics, 2019, 754, 73-79.	2.2	16
34	Connection between the Jurassic oceanic lithosphere of the Gulf of Cádiz and the Alboran slab imaged by Sp receiver functions. Geology, 2019, 47, 227-230.	4.4	11
35	Seismic, Receiver Function Technique. Encyclopedia of Earth Sciences Series, 2019, , 1-13.	0.1	0
36	A STEP fault in Central Betics, associated with lateral lithospheric tearing at the northern edge of the Gibraltar arc subduction system. Earth and Planetary Science Letters, 2018, 486, 32-40.	4.4	22

XIAOHUI YUAN

#	Article	IF	CITATIONS
37	Insight into the subducted Indian slab and origin of the Tengchong volcano in SE Tibet from receiver function analysis. Earth and Planetary Science Letters, 2018, 482, 567-579.	4.4	44
38	Continental lithospheric subduction and intermediate-depth seismicity: Constraints from S-wave velocity structures in the Pamir and Hindu Kush. Earth and Planetary Science Letters, 2018, 482, 478-489.	4.4	29
39	Crustal Radial Anisotropy and Linkage to Geodynamic Processes: A Study Based on Seismic Ambient Noise in Southern Madagascar. Journal of Geophysical Research: Solid Earth, 2018, 123, 5130-5146.	3.4	17
40	Seismic Anisotropy Beneath the Pamir and the Hindu Kush: Evidence for Contributions From Crust, Mantle Lithosphere, and Asthenosphere. Journal of Geophysical Research: Solid Earth, 2018, 123, 10,727.	3.4	13
41	Lateral Moho variations and the geometry of the Main Himalayan Thrust beneath the Nepal Himalayan orogen revealed by teleseismic receiver functions. Geophysical Journal International, 2018, 214, 1004-1017.	2.4	22
42	Seismic structure of the lithosphere beneath <scp>NW</scp> <scp>N</scp> amibia: Impact of the <scp>T</scp> ristan da <scp>C</scp> unha mantle plume. Geochemistry, Geophysics, Geosystems, 2017, 18, 125-141.	2.5	14
43	Detection of a new sub-lithospheric discontinuity in Central Europe with S-receiver functions. Tectonophysics, 2017, 700-701, 19-31.	2.2	21
44	Crustal structure of southern Madagascar from receiver functions and ambient noise correlation: Implications for crustal evolution. Journal of Geophysical Research: Solid Earth, 2017, 122, 1179-1197.	3.4	24
45	Tearing of the mantle lithosphere along the intermediateâ€depth seismicity zone beneath the Gibraltar Arc: The onset of lithospheric delamination. Geophysical Research Letters, 2017, 44, 4027-4035.	4.0	25
46	Detailed Configuration of the Underthrusting Indian Lithosphere Beneath Western Tibet Revealed by Receiver Function Images. Journal of Geophysical Research: Solid Earth, 2017, 122, 8257-8269.	3.4	54
47	Seismic anisotropy of the lithosphere and asthenosphere beneath southern Madagascar from teleseismic shear wave splitting analysis and waveform modeling. Journal of Geophysical Research: Solid Earth, 2016, 121, 6627-6643.	3.4	22
48	Deep India meets deep Asia: Lithospheric indentation, delamination and break-off under Pamir and Hindu Kush (Central Asia). Earth and Planetary Science Letters, 2016, 435, 171-184.	4.4	148
49	Receiver Functions with S Waves. , 2016, , 1-16.		1
50	Crustal thickness and <i>V_p</i> / <i>V_s</i> ratio in NW Namibia from receiver functions: Evidence for magmatic underplating due to mantle plumeâ€crust interaction. Geophysical Research Letters, 2015, 42, 3330-3337.	4.0	27
51	Depthâ€variant azimuthal anisotropy in Tibet revealed by surface wave tomography. Geophysical Research Letters, 2015, 42, 4326-4334.	4.0	46
52	Structure of the upper mantle in the north-western and central United States from USArray S-receiver functions. Solid Earth, 2015, 6, 957-970.	2.8	20
53	Thickness of the lithosphere beneath Turkey and surroundings from S-receiver functions. Solid Earth, 2015, 6, 971-984.	2.8	72
54	Anisotropic lowâ€velocity lower crust beneath the northeastern margin of <scp>T</scp> ibetan <scp>P</scp> lateau: Evidence for crustal channel flow. Geochemistry, Geophysics, Geosystems, 2015, 16, 4223-4236.	2.5	35

Χιαοήμι Υμάν

#	Article	IF	CITATIONS
55	Tearing of the Indian lithospheric slab beneath southern Tibet revealed by SKS-wave splitting measurements. Earth and Planetary Science Letters, 2015, 413, 13-24.	4.4	171
56	Is the Asian lithosphere underthrusting beneath northeastern Tibetan Plateau? Insights from seismic receiver functions. Earth and Planetary Science Letters, 2015, 428, 172-180.	4.4	41
57	Magmatic underplating and crustal growth in the Emeishan Large Igneous Province, SW China, revealed by a passive seismic experiment. Earth and Planetary Science Letters, 2015, 432, 103-114.	4.4	78
58	Mapping crustal structure beneath southern Tibet: Seismic evidence for continental crustal underthrusting. Gondwana Research, 2015, 27, 1487-1493.	6.0	63
59	Delamination of southern Puna lithosphere revealed by body wave attenuation tomography. Journal of Geophysical Research: Solid Earth, 2014, 119, 549-566.	3.4	23
60	A ubiquitous lowâ€velocity layer at the base of the mantle transition zone. Geophysical Research Letters, 2014, 41, 836-842.	4.0	32
61	Structure of the crust and the lithosphere beneath the southern Puna plateau from teleseismic receiver functions. Earth and Planetary Science Letters, 2014, 385, 1-11.	4.4	40
62	The Moho beneath western Tibet: Shear zones and eclogitization in the lower crust. Earth and Planetary Science Letters, 2014, 408, 370-377.	4.4	71
63	Shear wave splitting and shear wave splitting tomography of the southern Puna plateau. Geophysical Journal International, 2014, 199, 688-699.	2.4	10
64	Central Andean mantle and crustal seismicity beneath the Southern Puna plateau and the northern margin of the Chileanâ€Pampean flat slab. Tectonics, 2014, 33, 1636-1658.	2.8	42
65	A 3D shear-wave velocity model of the upper mantle beneath China and the surrounding areas. Tectonophysics, 2014, 633, 193-210.	2.2	40
66	Seismotectonics of the Pamir. Tectonics, 2014, 33, 1501-1518.	2.8	108
67	Deep burial of Asian continental crust beneath the Pamir imaged with local earthquake tomography. Earth and Planetary Science Letters, 2013, 384, 165-177.	4.4	91
68	Scandinavia: A former Tibet?. Geochemistry, Geophysics, Geosystems, 2013, 14, 4479-4487.	2.5	25
69	Teleseismic tomography of the southern Puna plateau in Argentina and adjacent regions. Tectonophysics, 2013, 586, 65-83.	2.2	76
70	Normal faulting from simple shear rifting in South Tibet, using evidence from passive seismic profiling across the Yadong-Gulu Rift. Tectonophysics, 2013, 606, 178-186.	2.2	34
71	Geometry of the Pamirâ€Hindu Kush intermediateâ€depth earthquake zone from local seismic data. Journal of Geophysical Research: Solid Earth, 2013, 118, 1438-1457.	3.4	156
72	Seismic imaging of subducting continental lower crust beneath the Pamir. Earth and Planetary Science Letters, 2013, 375, 101-112.	4.4	158

Χιαομυί Υυάν

#	Article	IF	CITATIONS
73	Velocity structure beneath the southern Puna plateau: Evidence for delamination. Geochemistry, Geophysics, Geosystems, 2013, 14, 4292-4305.	2.5	25
74	Seismic evidence for stratification in composition and anisotropic fabric within the thick lithosphere of Kalahari Craton. Geochemistry, Geophysics, Geosystems, 2013, 14, 5393-5412.	2.5	85
75	USArray Receiver Function Images of the Lithosphere-Asthenosphere Boundary. Seismological Research Letters, 2012, 83, 486-491.	1.9	68
76	Brief communication "Seismic and acoustic-gravity signals from the source of the 2004 Indian Ocean Tsunami". Natural Hazards and Earth System Sciences, 2012, 12, 287-294.	3.6	3
77	The lithosphere-asthenosphere boundary observed with USArray receiver functions. Solid Earth, 2012, 3, 149-159.	2.8	26
78	Locating the Tohoku-Oki 2011 tsunami source using acoustic–gravity waves. Journal of Seismology, 2012, 16, 215-219.	1.3	3
79	Crustal and uppermost mantle velocity structure along a profile across the Pamir and southern Tien Shan as derived from project TIPAGE wide-angle seismic data. Geophysical Journal International, 2012, 188, 385-407.	2.4	113
80	Tracking unilateral earthquake rupture by P-wave polarization analysis. Geophysical Journal International, 2012, 188, 1141-1153.	2.4	11
81	Seismic receiver functions and the lithosphere–asthenosphere boundary. Tectonophysics, 2012, 536-537, 25-43.	2.2	150
82	High-resolution image of the geometry and thickness of the subducting Nazca lithosphere beneath northern Chile. Journal of Geophysical Research, 2011, 116, .	3.3	38
83	Details of the Doublet Moho Structure beneath Lhasa, Tibet, Obtained by Comparison of P and S Receiver Functions. Bulletin of the Seismological Society of America, 2011, 101, 1259-1269.	2.3	18
84	Receiver function images of the base of the lithosphere in the Alboran Sea region. Geophysical Journal International, 2011, 187, 1019-1026.	2.4	18
85	Seismic, Receiver Function Technique. Encyclopedia of Earth Sciences Series, 2011, , 1258-1269.	0.1	2
86	Response of mantle transition zone thickness to plume buoyancy flux. Geophysical Journal International, 2010, 180, 49-58.	2.4	6
87	Receiver function summation without deconvolution. Geophysical Journal International, 2010, 180, 1223-1230.	2.4	41
88	Study of the lithospheric and upper-mantle discontinuities beneath eastern Asia by SS precursors. Geophysical Journal International, 2010, 183, 252-266.	2.4	25
89	Seismic Images of the Biggest Crash on Earth. Science, 2010, 329, 1479-1480.	12.6	66
90	The boundary between the Indian and Asian tectonic plates below Tibet. Proceedings of the National Academy of Sciences of the United States of America, 2010, 107, 11229-11233.	7.1	332

XIAOHUI YUAN

#	Article	IF	CITATIONS
91	Seismic signature of the collision between the east Tibetan escape flow and the Sichuan Basin. Earth and Planetary Science Letters, 2010, 292, 254-264.	4.4	203
92	The elusive lithosphere–asthenosphere boundary (LAB) beneath cratons. Lithos, 2009, 109, 1-22.	1.4	365
93	Receiver function images from the Moho and the slab beneath the Altiplano and Puna plateaus in the Central Andes. Geophysical Journal International, 2009, 177, 296-308.	2.4	48
94	Evidence for a missing crustal root and a thin lithosphere beneath the Central Alborz by receiver function studies. Geophysical Journal International, 2009, 177, 733-742.	2.4	79
95	The M w 3.1–4.7 earthquakes in the southern Baltic Sea and adjacent areas in 2000, 2001 and 2004. Journal of Seismology, 2008, 12, 413-429.	1.3	11
96	Upper mantle and lithospheric heterogeneities in central and eastern Europe as observed by teleseismic receiver functions. Geophysical Journal International, 2008, 174, 351-376.	2.4	40
97	Crustal thickness estimation beneath the southern central Andes at 30°S and 36°S from <i>S</i> wave receiver function analysis. Geophysical Journal International, 2008, 174, 249-254.	2.4	48
98	More constraints to determine the seismic structure beneath the Central Andes at 21°S using teleseismic tomography analysis. Journal of South American Earth Sciences, 2008, 25, 22-36.	1.4	40
99	Seismic evidence for widespread serpentinized forearc mantle along the Mariana convergence margin. Geophysical Research Letters, 2008, 35, .	4.0	47
100	Tracing the Hawaiian Mantle Plume by Converted Seismic Waves. , 2007, , 49-69.		5
101	An S receiver function analysis of the lithospheric structure in South America. Geophysical Research Letters, 2007, 34, .	4.0	96
102	Double seismic discontinuities at the base of the mantle transition zone near the Mariana slab. Geophysical Research Letters, 2007, 34, .	4.0	16
103	The rapid drift of the Indian tectonic plate. Nature, 2007, 449, 894-897.	27.8	391
104	The lithosphere-asthenosphere boundary beneath the western United States. Geophysical Journal International, 2007, 170, 700-710.	2.4	117
105	Imaging the colliding Indian and Asian lithospheric plates beneath Tibet. Journal of Geophysical Research, 2006, 111, n/a-n/a.	3.3	186
106	TheSreceiver functions: synthetics and data example. Geophysical Journal International, 2006, 165, 555-564.	2.4	191
107	Deep origin of the Hawaiian tilted plume conduit derived from receiver functions. Geophysical Journal International, 2006, 166, 767-781.	2.4	40
108	Lithospheric thickness beneath the Dabie Shan, central eastern China from <i>S</i> receiver functions. Geophysical Journal International, 2006, 166, 1363-1367.	2.4	64

Χιαομυί Υυάν

#	Article	IF	CITATIONS
109	Deep seismic images of the Southern Andes. , 2006, , .		18
110	Seismological Studies of the Central and Southern Andes. , 2006, , 443-457.		24
111	Receiver function images of the central Chugoku region in the Japanese islands using Hi-net data. Earth, Planets and Space, 2005, 57, 271-280.	2.5	24
112	The lithosphere–asthenosphere boundary in the North-West Atlantic region. Earth and Planetary Science Letters, 2005, 236, 249-257.	4.4	126
113	The lithosphere-asthenosphere boundary in the Tien Shan-Karakoram region from S receiver functions: Evidence for continental subduction. Geophysical Research Letters, 2005, 32, n/a-n/a.	4.0	147
114	Moho geometry and upper mantle images of northeast India. Geophysical Research Letters, 2005, 32, n/a-n/a.	4.0	44
115	Seismic monitoring of the Indian Ocean tsunami. Geophysical Research Letters, 2005, 32, .	4.0	41
116	Rejuvenation of the lithosphere by the Hawaiian plume. Nature, 2004, 427, 827-829.	27.8	233
117	Seismic Detection and Characterization of the Altiplano-Puna Magma Body, Central Andes. Pure and Applied Geophysics, 2003, 160, 789-807.	1.9	161
118	Receiver function study of the Hellenic subduction zone: imaging crustal thickness variations and the oceanic Moho of the descending African lithosphere. Geophysical Journal International, 2003, 155, 733-748.	2.4	82
119	Seismic observation of narrow plumes in the oceanic upper mantle. Geophysical Research Letters, 2003, 30, .	4.0	30
120	Seismic imaging of a convergent continental margin and plateau in the central Andes (Andean) Tj ETQq0 0 0 rgB1	[Qyerloc	k 10 Tf 50 30 128
121	Seismic study of upper mantle and transition zone beneath hotspots. Physics of the Earth and Planetary Interiors, 2003, 136, 79-92.	1.9	52
122	Receiver functions in northeast China – implications for slab penetration into the lower mantle in northwest Pacific subduction zone. Earth and Planetary Science Letters, 2003, 216, 679-691.	4.4	120
123	Seismic Detection and Characterization of the Altiplano-Puna Magma Body, Central Andes. , 2003, , 789-807.		5
124	Seismic Images of Crust and Upper Mantle Beneath Tibet: Evidence for Eurasian Plate Subduction. Science, 2002, 298, 1219-1221.	12.6	570
125	Moho topography in the central Andes and its geodynamic implications. Earth and Planetary Science Letters, 2002, 199, 389-402.	4.4	222
126	Receiver function analysis of the North American crust and upper mantle. Geophysical Journal International, 2002, 150, 91-108.	2.4	49

XIAOHUI YUAN

#	Article	IF	CITATIONS
127	Mapping the Hawaiian plume conduit with converted seismic waves. Nature, 2000, 405, 938-941.	27.8	174
128	Subduction and collision processes in the Central Andes constrained by converted seismic phases. Nature, 2000, 408, 958-961.	27.8	337
129	A detailed receiver function image of the upper mantle discontinuities in the Japan subduction zone. Earth and Planetary Science Letters, 2000, 183, 527-541.	4.4	79
130	Seismic Evidence for a Detached Indian Lithospheric Mantle Beneath Tibet. Science, 1999, 283, 1306-1309.	12.6	371
131	Lithospheric and upper mantle structure of southern Tibet from a seismological passive source experiment. Journal of Geophysical Research, 1997, 102, 27491-27500.	3.3	338
132	Evidence from Earthquake Data for a Partially Molten Crustal Layer in Southern Tibet. Science, 1996, 274, 1692-1694.	12.6	226